Proceedings of the ASME 2017 International Mechanical Engineering Congress and Exposition
IMECE2017
November 3-9, 2017, Tampa, Florida, USA

IMECE2017-71345

INPUT SHAPING FOR FLEXIBLE SYSTEM WITH NONLINEAR SPRING AND DAMPER

Withit Chatlatanagulchai
Department of Mechanical Engineering
Faculty of Engineering
Kasetsart University
Chatuchak, Bangkok, Thailand

Ittidej Moonmangmee
School of Science and Technology
Sukhothai Thammathirat Open University
Pakkret, Nonthaburi, Thailand

Pisit Intarawirat
Department of Mechanical Engineering
Faculty of Engineering
Kasetsart University
Chatuchak, Bangkok, Thailand

ABSTRACT

Input shaping suppresses residual vibration by destructive interference of the impulse responses. Because proper destructive interference requires superposition property of the linear system, traditional input shaper only applies to the linear flexible system. In this paper, the work and energy principle is used to derive input shaper for flexible system having nonlinear spring and damper. It was shown via simulation and experiment that this type of shaper performs well with nonlinear systems. Positive, robust, and negative input shapers are discussed.

INTRODUCTION

Residual vibration occurs at the end of the move when flexible system is moved rapidly from point to point. Ref. [1] proposed a so-called *Posicast* control to suppress the residual vibration. Posicast control is based on cancellation of responses of two impulses. Later on, [2] added more impulses to a so-called *Input Shaper* to provide more robustness to uncertainty in the mode parameters.

Because cancellation of impulse responses uses the superposition property, traditional input shaping only applies to linear and weakly nonlinear systems. Ref. [3] investigated the effectiveness of the input shaper on a configuration dependent nonlinear system that has two flexible modes. They concluded that even though some types of input shapers perform better than the others, the larger the variation in the system parameters, the less effective the shapers are.

A limited number of literature on input shaping for nonlinear flexible systems exists. Techniques that used phase portrait are in the following references. Ref. [4] designed a two-impulse input shaper for a type of nonlinear system using phase portraits. Ref. [5] applied the phase portrait method to design a two-impulse input shaper for flexible mechanical couplings with variable stiffness. Ref. [6] used the phase portrait of the payload oscillations to derive mathematical constraints. These constraints were then used to compute the switching times of the unity-magnitude input shaper.

Techniques that used linearization of the nonlinear system are in the following references. Ref. [7] proposed an adaptive input shaping method for nonlinear systems. The adaptive shaper adjusted the magnitudes and time locations of its impulses according to the instant frequency and damping of the linearized systems. Ref. [8] applied this adaptive shaper to suppression of payload swing in a three-dimensional overhead bridge crane with hoisting mechanism. Other works based on linearization of the nonlinear system are [9], using the method of multiple scales, and [10], where the linearization was applied to a parallel manipulator.

Other techniques on input shaping for nonlinear systems are in the following references. Ref. [11] applied the singular perturbation technique to a nonlinear multi-link flexible-link robot. The robot model was reduced to a slow, rigid-body

model and a fast, flexible-body model. A nonlinear feedback control was used to linearize and control the rigid-body model whereas an input shaper was used to suppress the residual vibration from the flexible-body model. Ref. [12] presented a sequential optimization technique for the design of input shapers for nonlinear systems. The nonlinear system is linearized about its nominal trajectories resulting in a series of linear programming problem. The linear programming problem solves for the necessary control effort to satisfy the boundary conditions and the state and control constraints. Ref. [13] considered movement of a rigid robot carrying a flexible payload. The modal excitation forces, which are the interaction forces from the robot to the payload, were shaped by the input shaper. Ref. [14] constructed the input as linear combinations of the first-order B-spline functions. The input was obtained from an optimization algorithm that allowed the use of nonlinear plant model and can be performed on-line. Ref. [15] applied the vector diagram approach to design a deflection-limiting velocity command for start-stop operation of a system having nonlinear actuators.

There is very little literature on input shaping design for nonlinear systems using work and energy principle. Ref. [16] and [17] considered the case when the spring stiffness is a configuration dependent nonlinear function. Principle of work and energy was applied to design input shapers in a displacement excitation and a force excitation problems. Ref. [18] applied the principle of work and energy to design a robust input shaper in a force excitation problem for a system with Duffing nonlinear spring stiffness.

In this paper, the work and energy principle is used to derive input shaper for flexible system having nonlinear spring and damper. The input shaper in this paper is based on the idea presented in [16] and [17]; its robust version is based on [18]. This paper, however, presents the following new features:

- Diagrams are used to clearly explain the displacement excitation problems. Formulas to obtain the input shaper are clearly derived. Various simulations are presented to illustrate the design.
- There is an experiment with a flexible-joint robot manipulator to show the practicality of this open-loop method in a closed-loop control system.
- The robust input shaper design is extended to a general *n*-impulse input shaper.
- Design of a negative input shaper using the work and energy principle is presented.

TWO-MASS RIGID-FLEXIBLE PLANT

Consider a two-mass rigid-flexible system with nonlinear spring and damper, as shown in Fig. 1. This system represents general two-degree-of-freedom flexible systems. $x_i, i=1,2,$ are absolute position coordinates of masses $m_i, i=1,2.$ m_1 is the rigid-body mass whose damping force is $F_0(\dot{x}_1)$ and control effort is u. m_2 is the flexible-body mass whose damping force is $F_c(\dot{x})$ and spring force is $F_k(x)$, where $x = x_2 - x_1$. The spring and damper forces are nonlinear functions of x_i and $\dot{x}_i$.

The equations of motion of the plant are

$$u - F_0(\dot{x}_1) + F_c(\dot{x}) + F_k(x) = m_1\ddot{x}_1,$$
$$-F_c(\dot{x}) - F_k(x) = m_2\ddot{x}_2. \quad (1)$$

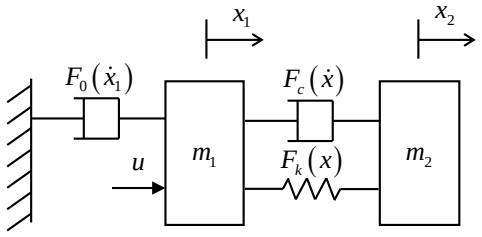

Fig. 1 Two-mass rigid-flexible plant with nonlinear spring and damper.

The objective is to design a reference signal, r_s, for the rigid-body mass, m_1, to follow so that both masses will arrive at a destination $x_1 = x_2 = x_d$ without residual vibration.

The closed-loop system under consideration is shown in Fig. 2, where *IS* is the input shaper, *C* is the controller, and *G* is the plant from the control effort to the positions of both masses. r_b is the baseline reference. r_s is the shaped reference. *e* is the tracking error. *u* is the control effort.

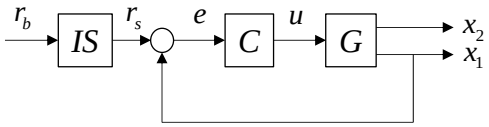

Fig. 2 Closed-loop system under consideration.

INPUT SHAPING BASED ON WORK AND ENERGY PRINCIPLE

To design the input shaper, *IS*, that will produce a desired reference signal, r_s, consider a diagram in Fig. 3. The coordinates x_1 and x_2 are measured from the equilibrium positions where the spring and damper are unstretched. In Fig. 3(a), both masses are at rest at their origins. In Fig. 3(b), the mass m_1 moves to the right by a distance A_1. The distance A_1 was pre-computed so that the mass m_2 will rest at the destination $x_2 = x_d$. In Fig. 3(c), the mass m_2 reaches the point $x_2 = A_1$ where the spring and damper change from compress to stretch. At this position, the mass m_2 attains maximum velocity, $\dot{x}_{2,\max}$. In Fig. 3(d), the mass m_2 reaches the destination and is at rest. The mass m_1 moves to the right by a distance $A_2 = x_d - A_1$. In Fig. 3(e), both masses are at rest at the destination, $x_1 = x_2 = x_d$.

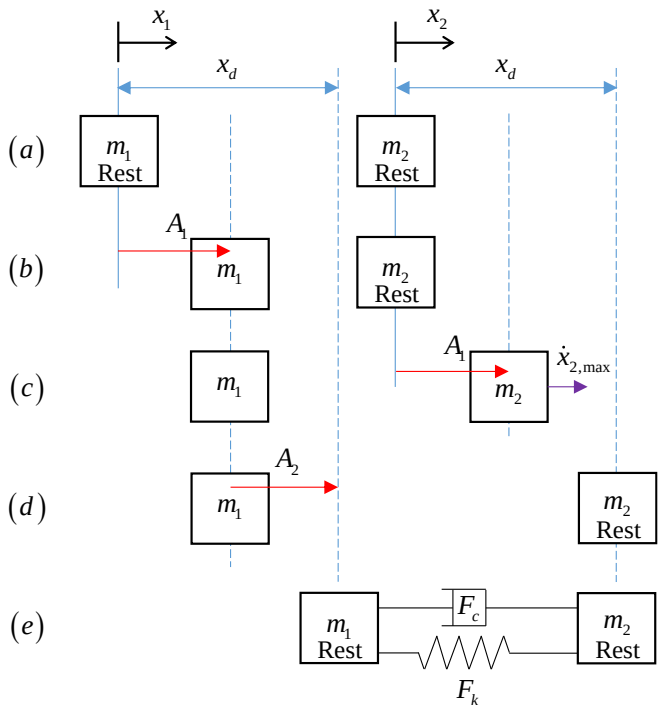

Fig. 3 Diagram of the two-mass system to design the input shaper.

A. Undamped System

For simplicity of exposition, undamped case $(F_c = 0)$ will be considered first. The distance A_1 can be computed from applying the work and energy principle to the mass m_2, moving from Fig. 3(b) to Fig. 3(d). From the work and energy principle,

$$\begin{aligned} U_{b\to d} &= T_d - T_b \\ -\int_{-A_1}^{x_d - A_1} F_k(x)\,dx &= 0 - 0, \end{aligned} \tag{2}$$

where $U_{b\to d}$ is the work by the spring force F_k to move the mass m_2 from Fig. 3(b) to Fig. 3(d) and T_d and T_b are the kinetic energy of the mass m_2 in Fig. 3(d) and Fig. 3(b), respectively. With a known spring force F_k, the distance A_1 can be obtained from solving (2).

The mass m_1 is required to move the distance A_2 at a time t_2, when the mass m_2 rests at the destination $x_2 = x_d$. To find the time t_2, applying the work and energy principle to the movement of the mass m_2 from point (b) to a general point x_2 yields

$$\begin{aligned} U_{b\to x_2} &= T_{x_2} - T_b \\ -\int_{-A_1}^{x_2 - A_1} F_k(x)\,dx &= \frac{1}{2} m_2 \dot{x}_2^2 - 0. \end{aligned} \tag{3}$$

Then, $\dot{x}_2$ can be solved from (3), and t_2 can be solved from

$$t_2 = \int_0^{x_d} \frac{1}{\dot{x}_2}\,dx_2. \tag{4}$$

For a linear spring, $F_k(x) = kx$, where k is a spring constant, (2) becomes

$$\left(\frac{1}{2}kA_1^2\right) - \left(\frac{1}{2}k\left(x_d - A_1\right)^2\right) = 0,$$

(3) becomes

$$\dot{x}_2 = \sqrt{\frac{kA_1^2 - k\left(x_2 - A_1\right)^2}{m_2}},$$

and (4) becomes

$$t_2 = \int_0^{x_d} \sqrt{\frac{m_2}{k\left(A_1^2\right) - k\left(x_2 - A_1\right)^2}}\,dx_2,$$

yielding $A_1 = x_d / 2$ and $t_2 = \pi / \sqrt{(k / m_2)}$. The resulting input shaper is exactly the ZV shaper.

For a nonlinear spring, traditional methods to obtain the input shaper based on the superposition principle do not apply; however, this proposed method based on the work and energy principle is applicable. As an example, considering the Duffing nonlinear spring $F_k(x) = k_1 x + k_2 x^3$, where k_1 and k_2 are spring constants, (2) still yields $A_1 = x_d / 2$, (3) results in

$$\dot{x}_2 = \sqrt{\frac{k_1 A_1^2 + 0.5k_2 A_1^4 - k_1\left(x_2 - A_1\right)^2 - 0.5k_2\left(x_2 - A_1\right)^4}{m_2}},$$

and (4) becomes

$$t_2 = \int_0^{x_d} \sqrt{\frac{m_2}{k_1 A_1^2 + 0.5k_2 A_1^4 - k_1\left(x_2 - A_1\right)^2 - 0.5k_2\left(x_2 - A_1\right)^4}}\,dx_2.$$

In simulation, let $k_1 = 10$, $k_2 = 100$, $m_2 = 1\,\text{kg}$, and $x_d = 1\,\text{m}$. The amplitude A_1 equals $x_d / 2 = 0.5\,\text{m}$. The time location t_2 of the second amplitude A_2 can be computed from the formula above as $t_2 = 0.5912\,\text{s}$. Fig. 4 shows the simulation result by simulating the equation of motion (1), relating x_1 to x_2. Fig. 4(a) shows the result when x_1 is moved to the right by an amplitude $A_1 = 0.5\,\text{m}$. The mass m_2 oscillates and reaches the first zero-velocity point, $x_2 = x_d = 1\,\text{m}$, at the time $t_2 = 0.5912\,\text{s}$, as computed. Fig. 4(b) shows the result when x_1 is moved further to the right by an amplitude $A_2 = 0.5\,\text{m}$ at the time location t_2. The mass m_2 stops oscillating, and both masses arrive at the destination $x_1 = x_2 = x_d = 1\,\text{m}$ without residual vibration.

B. Damped System

Normally, the result in the previous undamped section should also apply to systems with weakly damped. In the case when damping is substantial, finding A_1 and t_2 may require some approximations.

Consider a damped system with a damping force, $F_c(\dot{x})$. Eq. (2) becomes

$$U_{b\to d} = T_d - T_b$$
$$-\int_{-A_1}^{x_d - A_1} \left[F_k(x) + F_c(\dot{x}) \right] dx = 0 - 0, \tag{5}$$

and (3) becomes

$$U_{b\to x_2} = T_{x_2} - T_b$$
$$-\int_{-A_1}^{x_2 - A_1} \left[F_k(x) + F_c(\dot{x}) \right] dx = \frac{1}{2} m_2 \dot{x}_2^2 - 0.$$

For example, consider a nonlinear damper $F_c(\dot{x}) = c\dot{x}^3$, where c is a damping constant, and a nonlinear spring $F_k(x) = k_1 x + k_2 x^3$. Eq. (5) results in

$$\frac{1}{2}k_1 A_1^2 + \frac{1}{4}k_2 A_1^4 - \frac{1}{2}k_1 (x_d - A_1)^2 - \frac{1}{4}k_2 (x_d - A_1)^4 - \int_0^{t_2} c\dot{x}^3 \dot{x} dt = 0.$$

Because the time response, $x(t)$, is not known, the integral term above, which represents the dissipated energy due to the damper, cannot be computed. However this dissipated energy can be approximated by computing the energy dissipated in viscous damping, for a simple harmonic motion with $x(t) = x_d \sin \omega_d t$, as

$$\int_0^{t_2} c\dot{x}^3 \dot{x} dt \approx \int_0^{\frac{\pi}{2\omega_d}} c\dot{x}^4 dt = \int_0^{\frac{\pi}{2\omega_d}} c\left(x_d \omega_d \cos \omega_d t \right)^4 dt = c x_d^4 \omega_d^3 \left(\frac{3\pi}{16\omega_d} + \frac{\sin(\pi/\omega_d)}{4} + \frac{\sin(2\pi/\omega_d)}{32} \right),$$

where ω_d is the approximated oscillating frequency. Then, the amplitude A_1 can be computed.

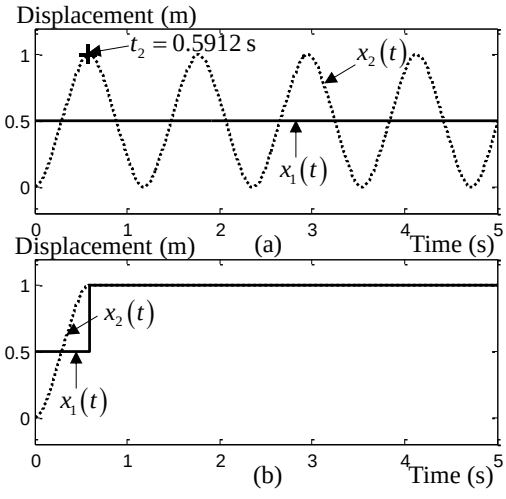

Fig. 4 Displacements x_1 (in the solid line) and x_2 (in the dotted line). (a) With the amplitude A_1. (b) With the amplitudes A_1 and A_2.

Another possibly more convenient way to find A_2 and t_2 by approximation is to use simulation or experimental results. As an example, consider a damping constant $c = 0.1$. Other plant parameters are the same as those in the undamped case. Fig. 5 contains the simulation result. In Fig. 5(a), the first amplitude A_1 can be found by trial and error until the maximum value of $x_2(t)$ equals the desired position, $x_d = 1$ m. The resulting A_1 is 0.525 m. The maximum value of $x_2(t)$ occurs at $t_2 = 0.5935$ s. Fig. 5(b) shows that both masses arrive at the desired position without residual vibration when both amplitudes, A_1 and A_2, are applied.

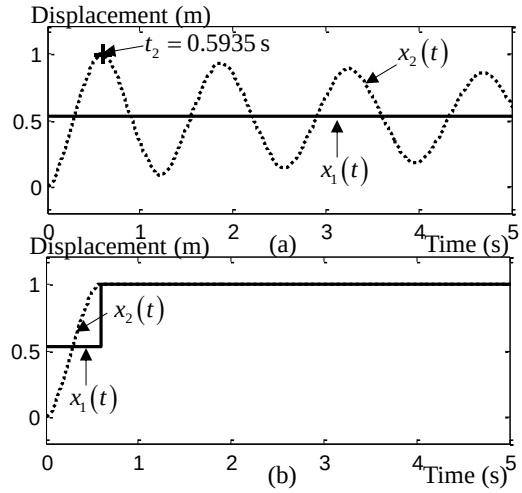

Fig. 5 Displacements x_1 (in the solid line) and x_2 (in the dotted line). (a) With the amplitude A_1. (b) With the amplitudes A_1 and A_2.

EXPERIMENT WITH A FLEXIBLE-JOINT ROBOT

In reality, the rigid-body mass, m_1, does not move exactly like the step function with amplitudes A_1 and A_2. Instead, the step function is used as a shaped reference input, r_s, for the mass m_1 to follow using the closed-loop system as shown in Fig. 2.

In this section, the proposed input shaping technique, based on work and energy principle, will be implemented with an actual flexible-joint robot to assess the practicality of the technique.

Consider a drawing of the flexible-joint robot, used in the experiment, as shown in Fig. 6. Encoder 1 measures the rigid-body motor shaft position, x_1. Encoder 2 measures the flexible-body link position, x_2. The two springs, positioned as shown, result in nonlinear spring forces, acting on the link. A National Instruments' Labview real-time system is used in real-time data acquisition and control.

Fig. 7 contains the motor shaft position, x_1, in the dotted line and the link position, x_2, in the solid line. Fig. 7 is analogous to Fig. 5(a). The difference is that, in reality, the motor shaft cannot have an abrupt step change in its magnitude.

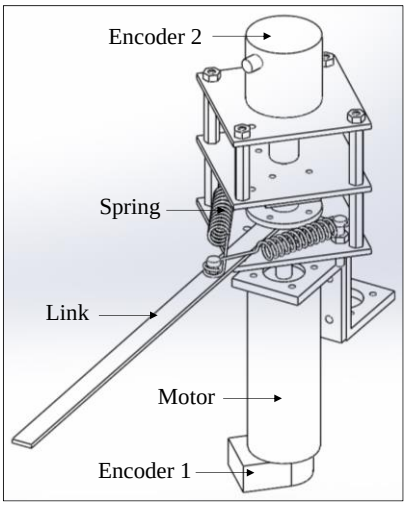

Fig. 6 Drawing of the flexible-joint robot in the experiment.

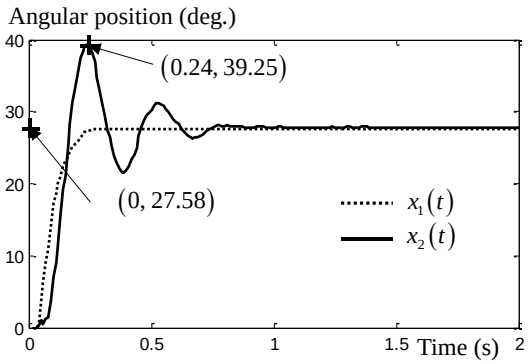

Fig. 7 Angular positions x_1 (in the dotted line) and x_2 (in the solid line).

From Fig. 7, the resulting input shaper, *IS*, has impulse amplitudes and time locations as

$$\begin{bmatrix} A_i \\ t_i \end{bmatrix} = \begin{bmatrix} \frac{27.58}{39.25} & \frac{(39.25-27.58)}{39.25} \\ 0 & 0.24 \end{bmatrix} = \begin{bmatrix} 0.703 & 0.297 \\ 0 & 0.24 \end{bmatrix}.$$

Note that the amplitudes of the two impulses are normalized so that the reference signals before and after the input shaper will have the same final value.

The feedback controller, *C*, in Fig. 2 was selected as a proportional controller with a gain $K_p = 0.02$. Fig. 8(a) shows the actual link angular position in degrees with and without the input shaper. Fig. 8(b) contains the link angular velocity in volts. The link angular velocity was measured by a gyroscope sensor. The input shaper substantially reduces the residual vibration for the flexible-joint robot.

ROBUST INPUT SHAPER

Parameters of the plant model can be uncertain. The uncertainty degrades the performance of the input shaper in suppressing the residual vibration. In general, more impulses can be added to the sequence to increase robustness of the input shaper at the expense of longer move time.

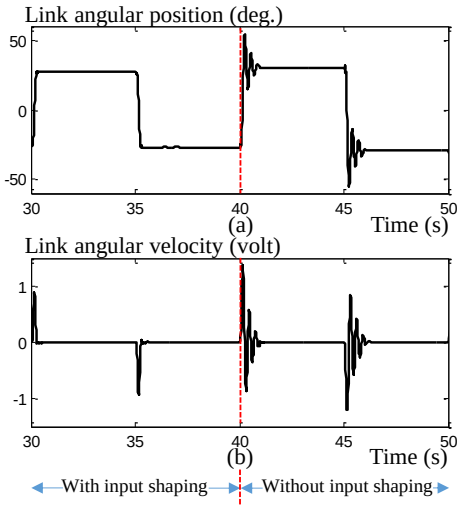

Fig. 8 (a) Link angular position. (b) Link angular velocity.

In the proposed method, adding more impulses is equivalent to adding resting points of the mass m_2 before the final resting point at $x_2 = x_d$. Fig. 9 contains a diagram of the robust input shaper by adding one impulse to the sequence. Fig. 9(d) shows the added resting point of the mass m_2. Note that Fig. 9(b) to Fig. 9(d) and Fig. 9(e) to Fig. 9(g) are equivalent to Fig. 3(b) to Fig. 3(d). Note also that, in Fig. 9(e), the movement of the mass m_1 begins immediately; therefore, the two impulses, A_{21} and A_{22}, are combined.

For an undamped system with zero damping force, $F_c = 0$, suppose there are *n* resting points at

$$0 = x_{d1} < x_{d2} < x_{d3} < \ldots < x_{dn} = x_d.$$

There will be *n* impulses in the input shaper sequence, whose amplitudes are

$$A_{12}, A_{21} + A_{22}, \ldots, A_{(n-1)1} + A_{(n-1)2}, A_{n1}$$

and time locations are

$$0 = t_1, t_2, t_3, \ldots, t_n.$$

From the work and energy principle, the amplitudes $A_{i2}, i = 1, 2, \ldots, n-1,$ can be found from solving

$$-\int_{x_{di}-(x_{di}+A_{12})}^{x_{d(i+1)}-(x_{di}+A_{12})} F_k(x)\,dx = 0, \tag{6}$$

and the amplitudes $A_{i1}, i = 2, 3, \ldots, n,$ are found from

$$A_{i1} = x_{di} - x_{d(i-1)} - A_{(i-1)2}. \tag{7}$$

The time locations, $t_i, i = 2, 3, \ldots, n,$ can be found from

$$t_i = t_{i-1} + \int_{x_{d(i-1)}}^{x_{di}} \frac{1}{\dot{x}_{2i}}\,dx_{2i}, \tag{8}$$

where $\dot{x}_{2i}$ can be solved from

$$-\int_{x_{d(i-1)}-\left(x_{d(i-1)}+A_{(i-1)2}\right)}^{x_{2i}-\left(x_{d(i-1)}+A_{(i-1)2}\right)} F_k(x)\,dx = \frac{1}{2}m_2\dot{x}_{2i}^2. \qquad (9)$$

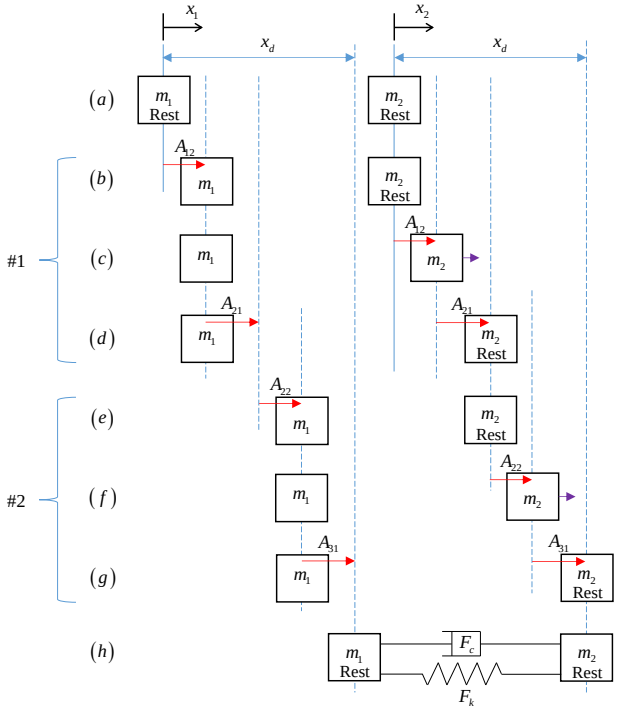

Fig. 9 Diagram of the two-mass system to design the robust input shaper.

For the Duffing nonlinear spring $F_k(x) = k_1x + k_2x^3$, where k_1 and k_2 are spring constants, (6) results in

$$A_{i2} = \frac{x_{d(i+1)} - x_{di}}{2},$$

and (9) yields

$$\dot{x}_{2i} = \sqrt{\frac{\begin{array}{l} k_1\left[x_{d(i-1)} - \left(x_{d(i-1)} + A_{(i-1)2}\right)\right]^2 \\ +0.5k_2\left[x_{d(i-1)} - \left(x_{d(i-1)} + A_{(i-1)2}\right)\right]^4 \\ -k_1\left[x_{2i} - \left(x_{d(i-1)} + A_{(i-1)2}\right)\right]^2 \\ -0.5k_2\left[x_{2i} - \left(x_{d(i-1)} + A_{(i-1)2}\right)\right]^4 \end{array}}{m_2}},$$

from which $t_i, i = 2, 3, ..., n,$ can be found using (8).

In simulation, using the same parameters as those for Fig. 4, choosing $x_{di}, i = 1, 2, ..., n,$ to be equally spaced, and letting the mass m_2 be 20% higher than its nominal value, Fig. 10 illustrates the robustness of the robust input shaper. The input shapers have 2, 4, and 6 impulses in Fig. 10(a), Fig. 10(b), and Fig. 10(c), respectively. Notice the lower residual vibration of the mass m_2 when more impulses are used in the input shaper at the expense of slower move time.

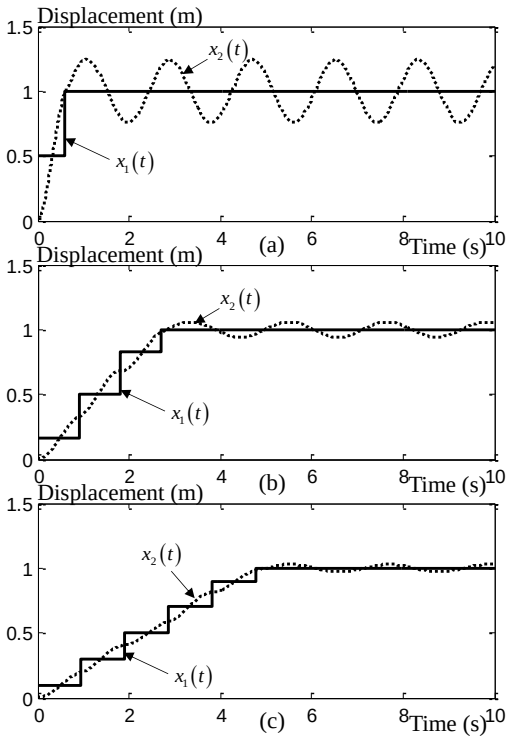

Fig. 10 Displacements x_1 (in the solid line) and x_2 (in the dotted line) when the mass m_2 is 20% higher than its nominal value. (a) With $n = 2$ impulses. (b) With $n = 4$ impulses. (c) With $n = 6$ impulses.

NEGATIVE INPUT SHAPER

An input shaper can have negative impulses, which will quicken the move time at the expense of instability due to excitation of high modes.

Consider a diagram of the unity-magnitude input shaper, shown in Fig. 11. In Fig. 11(b), the mass m_1 moves to the right by the desired distance, x_d. The mass m_2 is pushed to the right until it attains its maximum velocity, $\dot{x}_{2,\max}$; then, the mass m_1 is moved back to its origin to slow down the mass m_2. When the mass m_2 reaches its desired position with zero velocity, the mass m_1 is moved back to the right, so both masses are at rest at their desired positions.

Because the amplitudes of the impulses are known, only the time locations of the impulses are to be computed.

Consider an undamped case with the Duffing nonlinear spring $F_k(x) = k_1x + k_2x^3$, where k_1 and k_2 are spring constants. Applying the work and energy principle to the movement of the mass m_2 from point (b) to a general point x_2 results in

$$\begin{aligned} U_{b\to x_2} &= T_{x_2} - T_b \\ -\int_{-x_d}^{x_2-x_d} F_k(x)\,dx &= \frac{1}{2}m_2\dot{x}_2^2 - 0. \end{aligned} \qquad (10)$$

Eq. (10) is solved for $\dot{x}_2$ as

$$\dot{x}_2 = \sqrt{\frac{k_1 x_d^2 + 0.5 k_2 x_d^4 - k_1 \left(x_2 - x_d\right)^2 - 0.5 k_2 \left(x_2 - x_d\right)^4}{m_2}}.$$

The time location t_2 for the second impulse can be found from

$$t_2 = \int_0^{x_d/2} \frac{1}{\dot{x}_2} dx_2.$$

From symmetry, $t_3 = 2t_2$.

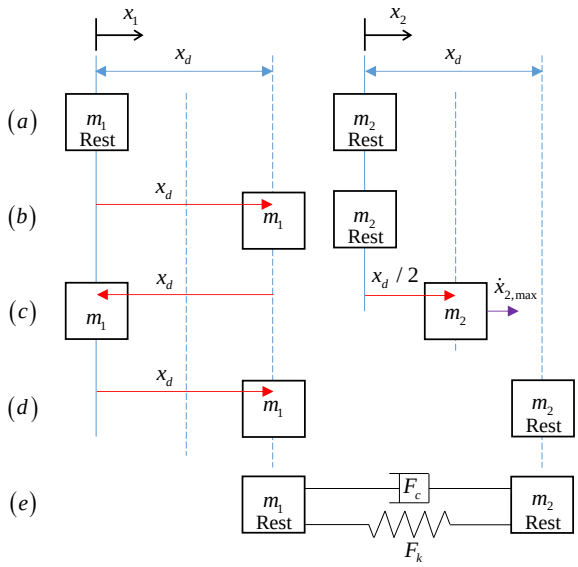

Fig. 11 Diagram of the two-mass system to design the negative input shaper.

Using the same simulation parameters as those for Fig. 4, the resulting negative input shaper is

$$\begin{bmatrix} A_i \\ t_i \end{bmatrix} = \begin{bmatrix} 1 & -1 & 1 \\ 0 & 0.1079 & 0.2158 \end{bmatrix}.$$

Fig. 12 contains the displacements of both masses. Both masses can reach their desired locations without residual vibration. Comparing the result in Fig. 12 to that of the positive input shaper in Fig. 4, both masses reach their desired locations quicker using the negative input shaper, that is, 0.5912 seconds using the positive input shaper and 0.2158 seconds using the negative input shaper.

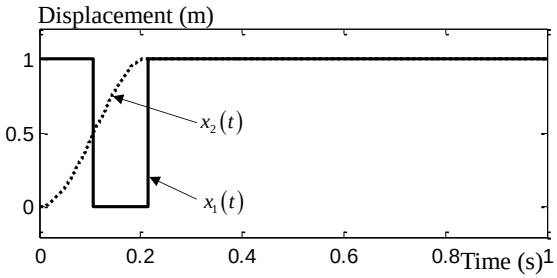

Fig. 12 Displacements x_1 (in the solid line) and x_2 (in the dotted line) using the negative input shaper.

CONCLUSIONS

This paper presents the design of input shapers using the work and energy principle. Unlike the superposition property that traditional input shapers are designed on, the work and energy principle still applies to nonlinear systems, and so do the designed input shapers.

The paper clearly illustrates the design process with simulations. An experiment with a flexible-joint robot shows the practicality of the proposed technique. The design covers a general *n*-impulse input shaper and a negative input shaper.

Being a technique for nonlinear systems, the amplitudes and time locations of the impulses are functions of plant model parameters, not the natural frequency and damping ratio. This opens up a new direction to which further research can be extended. Possible future research includes exploring the robustness property with respect to plant parameter variations, concurrent design with the feedback controller, and extending the result to multi-mode systems.

REFERENCES

[1] O. J. M. Smith, "Posicast control of damped oscillatory systems," *Proc. of the IRE*, vol. 45, no. 9, pp. 1249–1255, Sep. 1957.

[2] N. C. Singer and W. C. Seering, "Preshaping command inputs to reduce system vibration," *J. of Dynamic Systems, Measurement and Control*, vol. 112, no. 1, pp. 76–82, Mar. 1990.

[3] E. A. Crain, W. E. Singhose, and W. P. Seering, "Evaluation of input shaping on configuration dependent systems," in *Proc. 1996 Japan-USA Symposium on Flexible Automation*, Boston, MA, pp. 315–318.

[4] J. Park and C. B. Schrader, "Can an input shaper with two impulses suppress nonlinear residual vibrations?," in *Proc. ACC 2003*, Denver, CO, pp. 3172–3177.

[5] G. Pelaez, N. Cararrini, and J. C. Garcia-Prada, "Two-impulse sequence input shaper design for link mechanisms with nonlinearities," in *Proc. ACC 2007*, New York City, NY, pp. 822–827.

[6] Z. N. Masoud and M. F. Daqaq, "A graphical approach to input-shaping control design for container cranes with hoist," *IEEE Trans. on Control Systems Tech.*, vol. 14, no. 6, pp. 1070–1077, Nov. 2006.

[7] J. Stergiopoulos and A. Tzes, "Adaptive input shaping for nonlinear systems: a case study," *J. of Dynamic Systems, Measurement and Control*, vol. 129, no. 2, pp. 219–223, Mar. 2007.

[8] J. Stergiopoulos and A. Tzes, "An adaptive input shaping technique for the suppression of payload swing in three-dimensional overhead cranes with hoisting mechanism," in *Proc. IEEE ETFA 2007*, Patras, Greece, pp. 565–568.

[9] M. F. Daqaq and Z. N. Masoud, "Nonlinear input-shaping controller for quay-side container cranes," *Nonlinear Dynamics*, vol. 45, no. 1–2, pp. 149–170, Jul. 2006.

[10] K. Kozak, I. Ebert-Uphoff, and W. Singhose, "Locally linearized dynamic analysis of parallel manipulators and application of input shaping to reduce vibrations," *J. of Mechanical Design*, vol. 126, no. 1, pp. 156–168, Jan. 2004.

[11] F. Khorrami, S. Jain, and A. Tzes, "Experiments on rigid body-based controllers with input preshaping for a two-link flexible manipulator," *IEEE Trans. on Robotics and Automation*, vol. 10, no. 1, pp. 55–65, Feb. 1994.

[12] P. Singla, T. Singh, and S. G. Manyam, "Input shaping design using sequential linear programming (SLP) for non-linear systems," in *Proc. ACC 2008*, Seattle, WA, pp. 3275–3280.

[13] T. Zhou, A. A. Goldenberg, and J. W. Zu, "Modal force based input shaper for vibration suppression of flexible payloads," in *Proc. ICRA 2002*, Washington, DC, pp. 2430–2435.

[14] D. Gorinevsky and G. Vukovich, "Nonlinear input shaping control of flexible spacecraft reorientation maneuver," in *Proc. CCA 1996*, Dearborn, MI, pp. 970–975.

[15] Y.-U. Park, Y.-S. Min, and Y.-G. Sung, "Deflection-limiting commands with 1st-order actuators," in *Proc. ICCAS 2013*, Gwangju, Korea, pp. 1613–1617.

[16] J. Y. Smith, K. Kozak, and W. E. Singhose, "Input shaping for a simple nonlinear system," in *Proc. ACC 2002*, Anchorage, AK, pp. 821–826.

[17] K. C. Kozak, "Robust command generation for nonlinear systems," Ph.D. dissertation, Dept. Mech. Eng., Georgia Institute of Technology, Atlanta, GA, 2003.

[18] K.-S. Chen, T.-S. Yang, K.-S. Ou, and J.-F. Yin, "Design of command shapers for residual vibration suppression in Duffing nonlinear systems," *Mechatronics*, vol. 19, no. 2, pp. 184–198, Mar. 2009.